PAPER • OPEN ACCESS

Geometrical imaging accuracy, image quality and plan quality for prostate cancer treatments on a 1.5 T MRLinac in patients with a unilateral hip implant

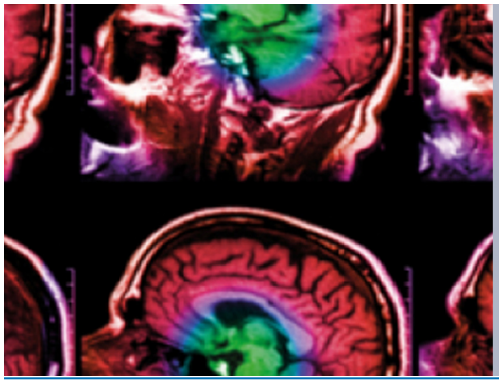

IOP Publishing Phys. Med. Biol. 66 (2021) 205013 https://doi.org/10.1088/1361-6560/ac1302

Physics in Medicine & Biology

IPEM Institute of Physics and Engineering in Medicine

OPEN ACCESS

RECEIVED
27 April 2021

REVISED
30 June 2021

ACCEPTED FOR PUBLICATION
9 July 2021

PUBLISHED
13 October 2021

PAPER

Geometrical imaging accuracy, image quality and plan quality for prostate cancer treatments on a 1.5 T MRLinac in patients with a unilateral hip implant

A L H M W van Lier, L T C Meijers, M E P Phillippens, J Hes, B W Raaymakers, J R N van der Voort van Zyp and J C J de Boer

University Medical Center Utrecht, Department of Radiotherapy, Utrecht, NL, The Netherlands

E-mail: a.l.h.m.w.vanlier@umcutrecht.nl

Keywords: MR-linac, geometrical accuracy, prostate, hip implant

Supplementary material for this article is available online

Abstract

Purpose. To assess the feasibility of prostate cancer radiotherapy for patients with a hip implant on an 1.5 T MRI-Linac (MRL) in terms of geometrical image accuracy, image quality, and plan quality. *Methods.* Pretreatment MRI images on a 1.5 T MRL and 3 T MRI consisting of a T2-weighted 3D delineation scan and main magnetic field homogeneity (B_0) scan were performed in six patients with a unilateral hip implant. System specific geometrical errors due to gradient nonlinearity were determined for the MRL. Within the prostate and skin contour, B_0 inhomogeneity, gradient nonlinearity error and the total geometrical error (vector summation of the prior two) was determined. Image quality was determined by visually scoring the extent of implant-born image artifacts. A treatment planning study was performed on five patients to quantify the impact of the implant on plan quality, in which conventional MRL IMRT plans were created, as well as plans which avoid radiation through the left or right femur. *Results.* The total maximum geometrical error in the prostate was <1 mm and the skin contour <1.7 mm; in all cases the machine-specific gradient error was most dominant. The B_0 error for the MRlinac MRI could partly be predicted based on the pre-treatment 3 T scan. Image quality for all patients was sufficient at 1.5 T MRL. Plan comparison showed that, even with avoidance of the hips, in all cases sufficient target coverage could be obtained with similar D1cc and D5cc to rectum and bladder, while V28Gy was slightly poorer in only the rectum for femur avoidance. *Conclusion.* We showed that geometrical accuracy, image quality and plan quality for six prostate patients with a hip implant or hip fixation treated on a 1.5 T MRL did not show relevant deterioration for the used image settings, which allowed safe treatment.

Introduction

The incidence of prostate cancer increases with age; therefore mainly elderly men are treated for this disease. In the current elderly population, hip implants (Kremers *et al* 2014) and hip fixation after a hip fracture are commonplace. Therefore, we see in our institute that a considerable portion of patients who are referred for prostate radiotherapy have a hip replacement or hip fixation device (hereafter generalized as 'hip implant'). In this study we report on our experience with, and workflow for radiotherapy treatment of this patient group on a 1.5 T MR-Linac (MRL).

The promise of an MRL treatment is improved precision by daily plan adaptation to target and organ-at-risk (OAR) position (Raaymakers *et al* 2017). Our initial experience shows that daily plan adaptation allows for margin reduction for prostate radiotherapy (de Muinck Keizer *et al* 2020). It was shown that IMRT plan quality on the MRL is equal to VMAT plans on a conventional machine for prostate treatments, including focal boosting (den Hartogh *et al* 2019).

Treating patients with a hip implant complicates the MRL treatment in three ways: (1) MR image geometrical accuracy may be reduced by the implant, (2) MRI image quality will be reduced by device-born image artifacts, (3) less flexibility in gantry angle choice to avoid irradiation through the device.

The geometrical accuracy of MR images depends on errors in the gradient system (machine dependent), and the static magnetic field (B_0) homogeneity. The gradient error is spatially dependent and using phantom measurements a 3D map of the error can be obtained. To illustrate, the near-maximum error (defined as 99th-percentile) caused by the residual gradient nonlinearity was reported to be 0.6–0.7 or 1.3–2.1 mm in a 150 or 350 mm diameter, respectively, in four evaluated MRL systems (Tijssen *et al* 2019). The residual gradient error is obtained after the scanner implemented correction on 3D images is performed. B_0 inhomogeneity can originate from machine imperfections (i.e. present without a patient in the scanner) or from local magnetic susceptibility variations (e.g. metallic implants have a higher magnetic susceptibility than tissue). In the current MRI scanners, the B_0 error is mainly caused by patient induced susceptibility alterations. To illustrate, on the same four MRL systems, in phantoms, a peak-to-peak B_0 error of 0.9 ppm was observed within a 350 mm diameter sphere. For a realistic readout bandwidth of 500 Hz mm^{-1}, this would translate in an geometrical error of 0.12 mm, which reflects the simulation with minimal susceptibility variations. In an another study, on the B_0 induced geometrical errors on an 1.5 T MRL in three patients with a hip implant the geometrical error due to B_0 inhomogeneity were estimated to be considerably larger within the prostate clinical tumor volume (CTV) with a maximum of approximately 0.35 mm (Keesman *et al* 2020). These larger errors were explained by the larger susceptibility difference between implant material and tissue, resulting in an inhomogeneous B_0 field. Based on these initial results we expect that the largest geometrical error originates from the gradient nonlinearity, though in situations where a hip implant is present, the B_0 inhomogeneity may give a relevant addition to the total error. However, given the limited number of patients included in the prior study, and the local nature of gradient nonlinearity and B_0 inhomogeneity further study into this topic is warranted.

In this study we report on total imaging geometrical accuracy, image quality and treatment plan quality in patients treated on the 1.5 T MR Linac (Unity, Elekta). We further investigated if a patient specific pretreatment 3 T MRI B_0 map can be used to predict the geometrical distortions on the 1.5 T MRL scan. Geometrical accuracy based both on patient-specific B_0 variations and machine-specific gradient nonlinearity will be taken into account.

Methods

Patient selection

Six consecutive patients eligible for external beam radiotherapy on the prostate using the 1.5 T MR linac (Unity, Elekta AB) with a unilateral hip implant or hip fixation device were analyzed (figure 1 and table 1). Patients were included between January and July 2020, during which period approximately 100 patients were treated for prostate cancer on the MRL.

Imaging and delineation

For all included patients, standard pre-treatment imaging was obtained which consists of a 3 T MRI scan session (Ingenia, Philips) including a B_0 map. In this B_0 map the deviation from the resonance frequency is measured using two spoiled gradient echo acquisitions with different echo time, all other settings were kept constant between the acquisitions. The difference between the phase images, corrected by the echo time spacing, is directly proportional to the off resonance. In our acquisition we chose to space our echo time such that we are minimally susceptible to the resonance difference between water and fat. The B_0 map was reconstructed on the scanner.

In addition, a CT scan ($1 \times 1 \times 3$ mm resolution, reconstruction with metal artifact reduction) was obtained as the presence of a metal in the field-of-view is a contra-indication for the MRonly workflow (Tyagi *et al* 2017) which would be our current standard for radiotherapy imaging workup for MRL treatments of the prostate. The CT scan is used to delineate the body contour and the bony structures.

Imaging was supplemented by a simulation MRL 1.5 T (Unity, Elekta) scan session to verify up-front the effect of the hip implant or fixation device on image quality and geometrical errors. For this purpose the clinical 3D T2-weighted workflow scan and a B_0 map were acquired. All scans were performed in treatment position. For all MRI scans, on both systems, B_0 shimming was performed using a standard implemented shimming option (called 'auto shim'), this shimming strategy is intended to optimize the B_0 homogeneity over the complete field of view. See table 2 for details on the scan protocol. All acquired scans are part of standard clinical work-up, retrospective use of clinical image data for this study was approved by our local medical ethical committee (20–519).

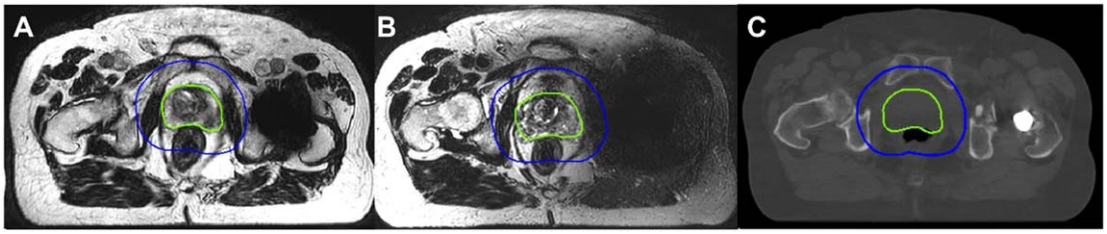

Figure 1. Example of image quality for (A) 1.5 T MRL workflow scan and (B) 3 T treatment planning scan. (C) CT scan with metal artifact reduction in reconstruction (window: 2500, level: 600) of patient 6 (left-sided total hip implant). For this particular case, the 1.5 T scan was scored as good image quality, while the 3 T MRL scan was scored as not good (i.e. limiting the ability to delineate structures around the prostate). This example also illustrates that in the current MRL workflow scan, the image artifact due to the implant is local, however, the true implant extent cannot accurately be determined.

Table 1. Implant characteristics and image quality score per patient. Image quality score: 1. Signal void in CTV 2. Signal void in PTV 3. Signal void within ring structure (1 cm om PTV) 4. Signal void within ring structure (2 cm om PTV) 5. No signal void within ring structure.

Patient	Implant type	Location	Image quality score 3 T	Image quality score 1.5 T
1	Total, non-metallic cup	L	5	5
2	Two fixation screws	R	5	5
3	Total, metallic cup	R	5	5
4	One fixation screw, rod in femur shaft	R	5	5
5	Total, non-metalic cup, with metallic wire	R	2	5
6	Total, non-metallic cup with metallic wire	L	3	5

The 3 T MRI image was delineated for planning purposes and an additional structure (named 'ring') was generated for further analysis purposes. The ring-structure was created by adding 2 cm anterior–posterior and left–right direction, and 1 cm in feet-head direction to the planning target volume (PTV). This structure is deemed appropriate for analysis purposes, as high dose levels and therefore all relevant structures for daily re-contouring and plan adaptation are encompassed in this volume. All 3 T and 1.5 T MRL images were registered using a rigid registration based on mutual information in a box around the prostate, which is part of our in-house developed multi-modality image viewer (Bol *et al* 2009). Prostate and ring delineations were transferred accordingly.

Our clinical workflow at the MRL is fully daily adaptive, meaning daily recontouring and plan optimization. Therefore, position of the body contour for the entrant beams is important as it directly relates to the radiological path length between beam entrance and target. We therefore examined the geometrical error within the first 3 mm skin as well.

Image quality

The presence of metallic implants directly affects the local B_0 field and therefore results in shorter local $T2^*$ and intra-voxel dephasing which ultimately leads to reduced local image intensity. Those problems can largely be circumvented using spin-echo sequences. However, off-resonances also result in problems with spin excitation and read-out (Lu *et al* 2009). Therefore, a signal void around the prosthesis is expected. Image quality is scored on the T2w images. We used a 5-point scoring system to quantify the signal void extent with respect to the relevant target volumes. The scoring was performed as followed (worst to best): 1. Signal void in CTV 2. Signal void in PTV 3. Signal void within ring structure (1 cm around PTV) 4. Signal void within ring structure (2 cm around PTV) 5. No signal void within ring structure.

Geometrical accuracy

The total geometrical accuracy is governed by residual gradient nonlinearity and B_0 inhomogeneity. Residual gradient nonlinearity errors is the remaining geometrical error, after correction which is incorporated on the image reconstructor. The residual gradient error is machine specific, while the magnetic susceptibility variations are induced by the patient. As surgical implants have a substantially different susceptibility compared to tissue, B_0 maps will show the effect of local susceptibility alterations by the implant. The total effect is a vector of the geometrical error over the three principal axis. The B_0 error only affects the frequency-encoding (read-out) direction for conventional 3D Cartesian sampling strategies.

For the analysis of the geometrical error it was split in three outcomes, namely: B_0 driven error, gradient driven error and total error. Geometrical errors for the 1.5 T MRL scan is given by: B_0 error (ΔB_0) , gradient nonlinearity error (ΔG) and total error (ΔT). ΔB_0 is based on patient specific B_0 maps, which are scaled to mm using bandwidth (BW) of 1.5 T T2 3D workflow scan

$$\Delta_{B_0\,\mathrm{mm}} = \Delta_{B_0\,\mathrm{Hz}}/\mathrm{BW}. \tag{1}$$

To determine the effect of ΔB_0 only, the absolute value of ΔB_0 will be calculated. The gradient nonlinearity error ΔG is machine-specific and derived from a vendor-supplied phantom measurement. From the measurements a 3D vector field is constructed which describes the spatial error in the three orthogonal directions (the two phase encoding and the frequency encoding direction: $\Delta_{G\ \mathrm{phase\ enc.}a}$, $\Delta_{G\ \mathrm{phase\ enc.}b}{}^2$, $\Delta_{G\ \mathrm{freq.enc.}}{}^2$, respectively), see for further details (Tijssen *et al* 2019). The absolute ΔG is derived using a vector summation:

$$\Delta_G = \sqrt{\Delta_{G\ \mathrm{phase\ enc.}a}{}^2 + \Delta_{G\ \mathrm{freq\ enc.}}{}^2 + \Delta_{G\ \mathrm{phase\ enc.}b}{}^2}. \tag{2}$$

To remove any B_0 effects from the measurement for the gradient nonlinearities, we repeated this measurement with opposing read-out direction, the average between the two measurements is used in this work. The gradient errors ($\Delta_{G\ \mathrm{phase\ enc.}a}$, $\Delta_{G\ \mathrm{phase\ enc.}b}$, $\Delta_{G\ \mathrm{freq.\ enc.}}$) are real valued; the sign gives the direction of the of the shift. As ΔB_0 only acts in the frequency encoding direction, the total error ΔT is given by:

$$\Delta_T = \sqrt{\Delta_{G\ \mathrm{phase\ enc.}a}{}^2 + (\Delta_{G\ \mathrm{freq.\ enc.}} + \Delta_{B_0\,\mathrm{mm}})^2 + \Delta_{G\ \mathrm{phase\ enc.}b}{}^2}. \tag{3}$$

In this case the real valued $\Delta_{B_0\,\mathrm{mm}}$ is used, such that the term ($\Delta_{G\ \mathrm{freq.\ enc.}} + \Delta_{B_0\,\mathrm{mm}}$) can show an additive (both terms are equal signed) or subtractive (terms are opposing signed) effect on the total error.

In our analysis we also compared the B_0 error specifically between the 1.5 and 3 T scan. Errors caused by magnetic susceptibility variations are theoretically twice as large in the 3 T scan as in the 1.5 T scan as the magnetization scales linearly with the applied magnetic field.

Prior to analysis any the patient-specific B_0 maps were unwrapped using an in-house implementation of a region-growing algorithm. The gradient error map is coarsely spaced at 25 × 25 × 55 mm resolution, which is the distance between the liquid markers in the gradient fidelity phantom (see (Tijssen *et al* 2019) for a description of the phantom). We interpolated this map using nearest-neighbor approach to the resolution of the B_0 map to stay close to the measurement results.

Treatment planning

To develop and evaluate a treatment planning strategy, we selected five prostate patients without prosthesis that had already been treated with SBRT on the MRL using a 7 field IMRT technique to deliver 5 × 7.25 Gy. We developed a treatment planning template in the Monaco TPS (5.40, Elekta AB) for hip prosthesis by avoiding, in each patient, either the left or the right hip, using identical dose prescriptions as for the case without prosthesis. From these 10 (5 left and 5 right) cases we obtained proper beam angles and sequencing parameters. Because we already had clinically delivered plans for these patients without prosthesis, we could directly assess possible plan degradation due to the more limited range of available beam angles. Details on MRL specific treatment planning considerations and applied constraints can be found in den Hartogh *et al* (2019), de Muinck Keizer *et al* (2020).

Results

Image quality

Image quality of the scan was deemed good, if the prosthesis induced an image artefact which did not extend into the delineation ring structure (i.e. image quality score of 5). Overall, image quality was good in 4/6 on 3 T and 6/6 patients on the 1.5 T MRL (see table 1). The signal void in the 3 T scan was always of larger extent than of the 1.5 T MRL scan. The signal void on the 1.5 T MRL scan does extend outside the real contour of the implant as was visualized on CT. This was particularly true for the total hip replacements (figure 1). In case of a hip fixation device, the difference between the MRL signal void and CT-observed device extent was smaller.

Geometrical accuracy

Despite phase wraps, we were able to obtain continuous B_0 maps after unwrapping in all patients (supplementary figure 1 (available online at stacks.iop.org/PMB/66/205013/mmedia)). Therefore we could directly quantify the B_0 error (ΔB_0). Only close to the hip implant the B_0 inhomogeneity could not be determined due to signal voids caused by the implant. An illustration of spatial distribution of the B_0 error (ΔB_0) , gradient error (ΔG) and total error (ΔT) is given in figure 2. The overall mean and mean of highest and lowest 2% voxels within the ring structure and skin was determined for all patients (figure 3). The largest mean of highest 2% observed in a patient was 0.6, 1.0 mm and 1.7 mm for PTV, ring and skin, respectively. The total error (largest of highest 2%) in the AP direction only, the most critical direction for correct delineation of the

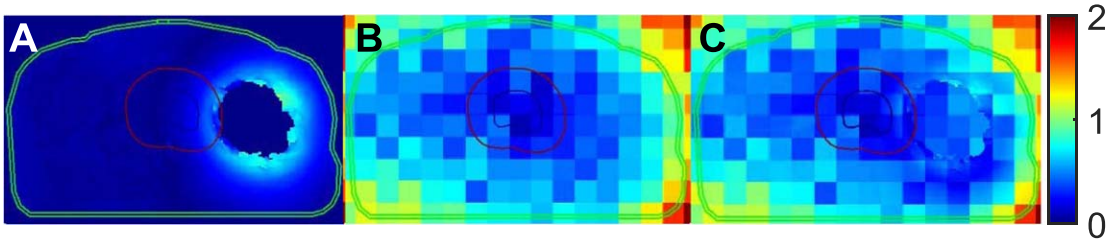

Figure 2. Geometrical error map for patient 6 (left-sided total hip implant) in millimeters. (A) B_0 inhomogeneity component (ΔB_0), (*B*) residual gradient error component (ΔG), or (C) total error (ΔT). Close to the hip implant the B_0 inhomogeneity could not be determined due to low signal intensity. The PTV (blue), ring (purple) and skin (green) contours are displayed in all images.

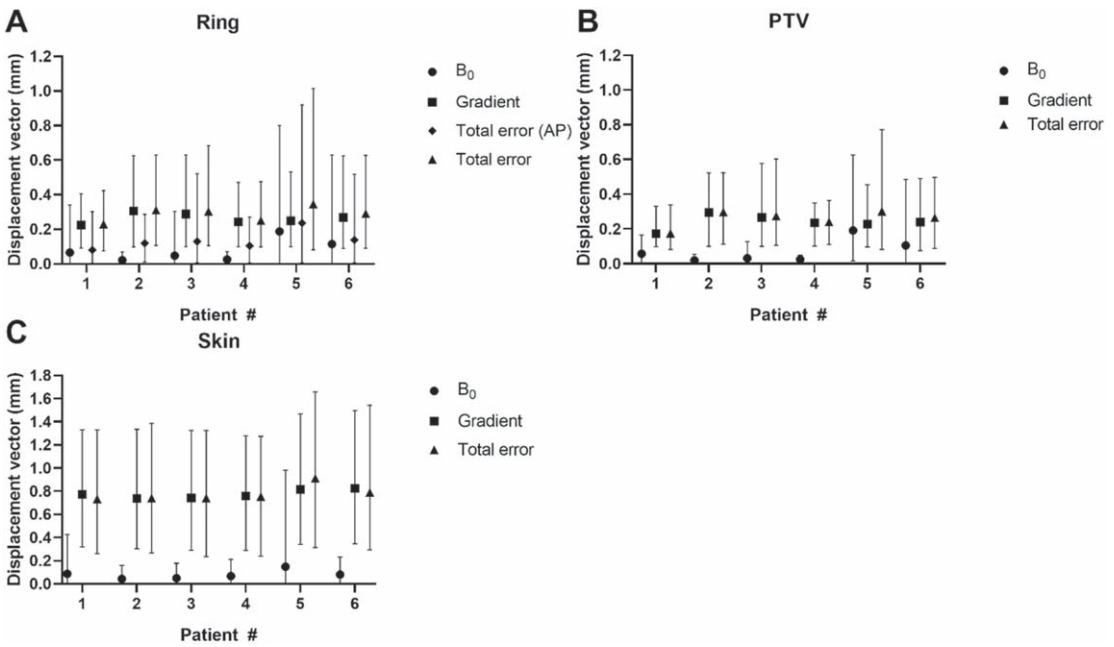

Figure 3. Geometrical error within the ring structure, PTV and skin. The total error (ΔT) is given, as well as the errors caused by the B_0 inhomogeneity (ΔB_0, absolute value) and the residual gradient error (ΔG). For the ring structure, separately the total error acting in the anterior–posterior (AP, read-out) direction is given, this is the most critical error with respect to OAR (bladder and rectum) delineation; this error is the sum of the AP component of the gradient error and the B_0 error. Per patient the mean as well as the mean of the lowest and highest 2% voxels are given. The residual gradient error is only machine-dependent and determined by the location of delineated structures with respect to the machine isocenter. The B_0 errors are patient specific.

rectum and bladder, was 0.9 mm in the ring. In all patients, but patient 5, the total error in the ring and skin was predominately governed by the machine-depend gradient error. In those patients the additive effect of ΔB_0 on top of ΔG to ΔT was less than 0.1 mm, while for patient 5 the additive effect was 0.5 mm.

To evaluate the predictive value of B_0 mapping at 3 T in the pre-treatment workup, ΔB_0 was also determined on the 3 T scan. For comparison, the observed values at 3 T were scaled with a factor 0.5 to correct for the theoretical difference between 1.5 T and 3 T susceptibility differences (figure 4). In patients 1–4 the 3 T scan were in line or overestimated the effect of ΔB_0 compared to the MRL 1.5 T scan. In patients 5–6 the 3 T scan underestimated the effect. In those two cases the ΔB_0 was largest.

Treatment planning

We found that a 7-field IMRT technique provided a robust and sufficient planning template (see suppl. figure 2 for a dose distribution).

The default set of gantry angles for a left-sided prosthesis were [30°, 135°, 160°, 225°, 260°, 290°, 350°], and the left–right mirrored values for a right sided prosthesis. Hence, the forbidden 'gap' due to a prosthesis was approximately 100° wide. This presented no problem for creating appropriate plans, since all constraints for both PTV and OAR were still well met. In particular, there was no deterioration when compared to the plans without prosthesis for high dose values in rectum (D1cc) and bladder (D5cc) (suppl. table 1). Lower dose values such as V28Gy increased slightly for rectum (on average 2% higher) but not for bladder. The intact femoral head

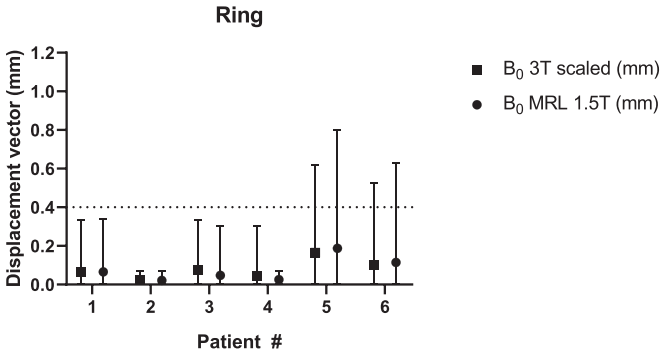

Figure 4. B_0 inhomogeneity (ΔB_0, absolute value) given as absolute displacement in the ring structure as observed on 3 T versus 1.5 T MRL. For the 3 T data an additional scaling of factor of 0.5 is applied to correct for the theoretical difference between 1.5 and 3 T susceptibility differences. Mean, mean of lowest 2% and mean of higher 2% are given per patient.

received a slightly higher dose, but the V28Gy was $<$ 0.3% in all cases. The number of monitor units and number of segments for prosthesis plans did not significantly increase with respect to the clinically delivered plans without prosthesis. Adding more beam directions yielded no significant improvements in the DVH parameters of the bladder and rectum.

Discussion

In this work, we scored image quality and quantified the total geometrical error for patients with a hip implant or hip fixation device referred for MR-guided radiotherapy treatment on the prostate. Furthermore, we looked at the achievable treatment planning quality for this patient category, taking into account the restriction that beam entrance through the implant should not take place.

In the study population, we found that the total geometrical error is governed by the residual gradient error. This means that for these cases the total geometrical error could be attributed to the implant, and that the geometrical error is similar in patients without an implant. This was true for the PTV, the ring used for on-line treatment plan optimization and for the relevant body contour. One exception was found, namely patient 5. Most likely the cause of this outlier is the specific prosthesis type, as other parameters such as location and volume of the ring and skin structure were similar to other patients. However, we do not have direct information on the implant type and had only CT available to judge the implant.

The additional error due to ΔB_0 in the body contour was always found at the ipsilateral side of the implant, which coincided with the omitted range of gantry angles. Therefore, the larger geometrical inaccuracy of the body contour seen in patient 5, does not impact dosimetric accuracy, as no beams enter through this part of the body. Looking to the future use of VMAT on the 1.5 T MRL systems, it remains advisable to still work with avoidance of gantry angles not only to prevent problems with body contour definition (which might be judged as minimal), but mainly due to problems with implant visualization.

In the current MR scans the exact shape of the implant is not properly visualized. Though a CT scan might be useful to delineate the implant pretreatment, the lack of image quality around the implant will hamper daily redelineation. Therefore, strategies in which the implant is defined daily in the treatment planning system using density overrides cannot be performed correctly. For safety purposes, we completely omit density overrides of the implant at the moment to prevent incorrect beam attenuation calculation. Although TSE sequences are already quite inert to metal artifacts, using the signal void as representation of the implant volume in those scans would lead to an overestimation of the volume. Therefore the attenuation correction would be too large which poses a risk of overdosage. Implementation of MRI techniques aimed at metal artifacts reduction (Lu *et al* 2009), which can be accelerated to be scanned in clinically reasonable scan times (Fritz *et al* 2016), may be required for this purpose. As an extension to those methods, it has been shown that from the shape of the signal void the actual implant extend can be estimated, allowing for an accurate of the implant geometry description (Shi *et al* 2017). Proper definition of implants on MRI may also pave the way for accurate pseudoCT scans in those patients, and thereby allowing an MRI-only workflow (Maspero *et al* 2017, Tyagi *et al* 2017, Kemppainen *et al* 2019).

The presented B_0 error is scaled to the read-out bandwidth of the workflow scan, therefore translating the presented results for a scan with a lower read-out bandwidth should be done with caution. However, it is anticipated that the measured B_0 is independent of the used treatment strategy (e.g. IMRT or VMAT) given that the magnetic field homogeneity is only very mildly affected by static and continuously rotating gantry positions, as well as multi-leaf motion (Jackson *et al* 2019, Kontaxis *et al* 2021).

Table 2. Image parameters of pre-treatment 3 T scans and 1.5 T MRL scans. All scans were reconstructed with the vendor-implemented 3D gradient nonlinearity correction enabled.

Scan	1.5 T MRL B_0 map	3 T B_0 map	1.5 T MRL workflow scan	3.0 T Treatment planning scan
Technique	3D, dual acquisition, spoiled gradient echo	3D, dual acquisition, spoiled gradient echo	3D T2w fast spin echo	3D T2w fast spin echo
Reconstructed resolution (mm^3)	1.85/1.85/2	2.0/2.0/1.5	0.8/0.8/2.0	0.8/0.8/2.0
TR/TE(/TE2)(ms)	11/4.6/9.2	9.6/4.6/6.9	1535/90	2500/356
Bandwidth (Hz mm^{-1})	390	467	496	257
Read-out direction	Anterior–posterior	Anterior–posterior	Anterior–posterior	Anterior–posterior

TR: repetition time, TE: echo time, TE2: second echo time, MRL: MRI-Linac.

In the work described here, all patients received a simulation 1.5 T MRL scan prior to treatment. Ideally, a simulation scan should not be required, as it results in extra patient burden and scan time on a treatment machine. Comparison in this small patient cohort showed that implant-born artifacts were smaller on the 1.5 T MRL than on the 3 T scan. Furthermore, the observed ΔB_0 at the 3 T scanner was related to the observed ΔB_0 at the 1.5 T MRL system. However, for the implants which have a larger estimated ΔB_0 (patient 5–6), the 3 T scan would underestimate the error at the 1.5 T system. Potentially, a more localized shimming approach could be used to circumvent this problem, and further improve B_0 homogeneity in and around the prostate. However, this approach relies on manually setting shim volume and may therefore result in user-dependent variations. Furthermore, the effect of this shim strategy on the B_0 homogeneity of the body contour will theoretically be less optimal.

Therefore, for future patients, we prescribe that if the estimated $\Delta B_0 < 0.4$ mm in the ring structure and/or a nonrelevant image artifact is seen at 3 T, no 1.5 T MRL simulation scan is required. While for a $\Delta B_0 > 0.4$ mm and/or relevant image artifact at 3 T an additional simulation scan is indicated to verify geometrical accuracy and image quality upfront. Always using a 1.5 T scan for simulation purposes in patients with an hip implant is also an option, although the reduced image artifacts at 1.5 T should be balanced with the general superiority of 3 T image quality, especially if the images are also used for diagnostic purposes (Barrett *et al* 2015).

For completeness, as can be seen in figure 3(A), a larger ΔB_0 does not necessarily lead to an increased ΔT. This can be best observed in the total error in AP direction. For example in patient 1, a mild ΔB_0 leads to a larger effect on ΔT, than the larger ΔB_0 for patient 6. In this case for patient 1 ΔB_0 is additive to the preexisting ΔG, while for patient 6 it is subtractive to ΔG.

Conclusions

We showed that for six consecutively scanned prostate cancer patient with a unilateral hip implant or hip fixation treated on a 1.5 T MRL geometrical accuracy, image quality and plan quality does not shown relevant deterioration. Pretreatment 3 T MR imaging can be used to verify these factors patient-specifically, and select individual cases for which an 1.5 T MRL simulation session upfront is indicated.

ORCID iDs

A L H M W van Lier https://orcid.org/0000-0002-2150-9776

References

Barrett T, Turkbey B and Choyke P L 2015 PI-RADS version 2: What you need to know *Clin. Radiol.* **70** 1165–76
Bol G H, Kotte A N T J, van der Heide U A and Lagendijk J J W 2009 Simultaneous multi-modality ROI delineation in clinical practice *Comput. Methods Prog. Biomed.* **96** 133–40
de Muinck Keizer D M *et al* 2020 Prostate intrafraction motion during the preparation and delivery of MR-guided radiotherapy sessions on a 1.5T MR-Linac *Radiother. Oncol.* **151** 88–94
den Hartogh M D *et al* 2019 Planning feasibility of extremely hypofractionated prostate radiotherapy on a 1.5 T magnetic resonance imaging guided linear accelerator *Phys. Imaging Radiat. Oncol.* **11** 16–20
Fritz J *et al* 2016 Compressed sensing SEMAC: 8-fold accelerated high resolution metal artifact reduction MRI of cobalt-chromium knee arthroplasty implants *Invest. Radiol.* **51** 666–76
Jackson S, Glitzner M, Tijssen R H N and Raaymakers B W 2019 MRI B 0 homogeneity and geometric distortion with continuous linac gantry rotation on an Elekta Unity MR-linac *Phys. Med. Biol.* **64** 0–7
Keesman R, van der Bijl E, Janssen T M, Vijlbrief T, Pos F J and van der Heide U A 2020 Clinical workflow for treating patients with a metallic hip prosthesis using magnetic resonance imaging-guided radiotherapy *Phys. Imaging Radiat. Oncol.* **15** 85–90
Kemppainen R *et al* 2019 Assessment of dosimetric and positioning accuracy of a magnetic resonance imaging-only solution for external beam radiotherapy of pelvic anatomy *Phys. Imaging Radiat. Oncol.* **11** 1–8
Kontaxis C, Woodhead P L, Bol G H, Lagendijk J J W and Raaymakers B W 2021 Proof-of-concept delivery of intensity modulated arc therapy on the Elekta Unity 1.5 T MR-linac *Phys. Med. Biol.* **66** 04LT01
Kremers H M *et al* 2014 Prevalence of total hip and knee replacement in the United States *J. Bone Joint Surg.* **97** 1386–97
Lu W, Pauly K B, Gold G E, Pauly J M and Hargreaves B A 2009 SEMAC: SLICE encoding for metal artifact correction in MRI *Magn. Reson. Med.* **62** 66–76
Maspero M *et al* 2017 Feasibility of MR-only proton dose calculations for prostate cancer radiotherapy using a commercial pseudo-CT generation method *Phys. Med. Biol.* **62** 9159–76
Raaymakers B W *et al* 2017 First patients treated with a 1.5 T MRI-Linac: Clinical proof of concept of a high-precision, high-field MRI guided radiotherapy treatment *Phys. Med. Biol.* **62** L41–50
Shi X, Yoon D, Koch K M and Hargreaves B A 2017 Metallic implant geometry and susceptibility estimation using multispectral B0 field maps *Magn. Reson. Med.* **77** 2402–13
Tijssen R H N *et al* 2019 MRI commissioning of 1.5T MR-linac systems - a multi-institutional study *Radiother. Oncol.* **132** 114–20
Tyagi N *et al* 2017 Clinical workflow for MR-only simulation and planning in prostate *Radiat. Oncol.* **12** 1–12